B4(XQ3)LYP-APPROACH

METHODOLOGY

3

In this chapter the details of the development of the B4(XQ3)LYP approach for the calculation of the redox potentials of transition metal complexes (TMC) will be represented. The chapter begins with the description of the computational methods followed by the presentation of results, discussion and conclusion.

3.1 Computational methodology

3.1.1 Model compounds

In this work a total of 48 4- and 6-coordinated TMCs were considered, including iron, manganese and nickel with diverse inorganic and organic ligands. The chemical structures of the ligands involved in considered TMCs can be found in the Table A1 of the Appendix section. Figures representing the three-dimensional structures of all considered compounds are also available in the Appendix (Figure A1). The TMCs were divided into two parts, namely:

1) 30 compounds (with 38 measured redox potentials by considering different solvents and redox states) for the **training set** to determine the parameters (Table 1) and
2) 18 compounds (with 20 measured redox potentials by considering different solvents and redox states) for the **prediction set** (Table 2).

Table 1. Training set of 30 different TMCs for which redox reactions are considered in three different solvents [water (W), acetonitrile (AN), dimethylformamide (DMF)].

No.[a]	model compound[b]	solvent[c]	No.[a]	model compound[b]	solvent[c]
1.	$[Fe(CN)_6]^{3-/4-}$	**W**	**17.**	$[Fe(PaPy_3)(AN)]^{2+/1+}$	**AN**
2.	$[Fe(bpy)_3]^{3+/2+}$	**W,AN,DMF**	**18.**	$[Fe(PaPy_3)(Cl)]^{1+/0}$	**AN**
3.	$[Fe(bpy)_2(CN)_2]^{1+/0}$	**W**	**19.**	$[Fe(PaPy_3)(N_3)]^{1+/0}$	**AN**
4.	$[Fe(phen)_3]^{3+/2+}$	**W,AN,DMF**	**20.**	$[Fe(PaPy_3)(CN)]^{1+/0}$	**AN**
5.	$[Fe(diammac)]^{3+/2+}$	**W**	**21.**	$[Fe(PaPy_2O)(Cl)]^{0/1-}$	**DMF**
6.	$[Fe(sar)]^{3+/2+}$	**W**	**22.**	$[Fe(SEt)_4]^{1-/2-}$	**AN**
7.	$[Fe(tacn)_2]^{3+/2+}$	**W**	**23.**	$[Fe(S_2\text{-o-xyl})_2]^{1-/2-}$	**DMF**
8.	$[Fe(PyIm_2H_2)_2]^{3+/2+}$	**AN**	**24.**	$[Fe(SEtOH)_4]^{1-/2-}$	**W**
9.	$[Fe(PyIm_2)_2]^{1-/2-}$	**AN**	**25.**	$[Mn(CN)_6]^{3-/4-}$	**W**
10.	$[Fe(PypepO)_2]^{1-/2-}$	**DMF**	**26_i.**	$[Mn(bpia)(Cl)_2]^{2+/1+}$	**AN**
11.	$[Fe(PypepS)_2]^{1-/2-}$	**DMF**	**26_{ii}.**	$[Mn(bpia)(Cl)_2]^{1+/0}$	**AN**
12.	$[Fe(PyAS)_2]^{1+/0}$	**DMF**	**27_i.**	$[Mn(py_2(NMe)_2)(Cl)_2]^{2+/1+}$	**AN**
13[d]**.**	$[Fe(bpteta)_2]^{3+/2+}$	**AN**	**27_{ii}.**	$[Mn(py_2(NMe)_2)(Cl)_2]^{1+/0}$	**AN**
14.	$[Fe(DITim)_2]^{1+/0}$	**AN**	**28.**	$[Mn(bpteta)]^{3+/2+}$	**AN**
15.	$[Fe(Pypep)_2]^{1+/0}$	**W,AN,DMF**	**29.**	$[Ni(bpy)]^{3+/2+}$	**W**
16.	$[Fe(Prpep)_2]^{1+/0}$	**W**	**30.**	$[Ni(bpteta)]^{3+/2+}$	**AN**

[a] Numbers in front are used to refer to specific TMCs in text.

[b] The total charges of the pairs of redox states are given as superscripts; for some TMCs (**26**, **27**) the redox potential is measured for two different pairs of redox states; a complete list of the structure of ligands is given in table S1 of the supplementary material; abbreviations for ligands: **AN**=acetonitrile; **bpy**=2,2'-bipyridinyl; **phen**=1,10-phenanthroline; **diammac**= 6,13-dimethyl-1,4,8,11-tetraazacyclotetradecane-6,13-diamine; **sar**=3,6,10,13,16,19-hexaaza-bicyclo[6.6.6]icosane; **tacn**=1,4,7-triazonane; **$PyIm_2$**=2,6-di-(1*H*-imidazol-2-yl)-pyridine-11,16-diide; **PypepO**=*N*-(2-hydroxyphenyl)pyridine-2-carboxamide-7,8-diide; **PypepS**=*N*-(2-mercaptophenyl)pyridine-2-carboxamide-7,8-diide; **PyAS**= 2-[(pyridin-2-ylmethylene)-amino]-benzenethiol-15-ide; **bpteta**=*N*-pyridin-2-ylmethyl-*N*'-(2-{2-[(pyridin-2-ylmethyl)-amino]-ethylamino}-ethyl)-ethane-1,2-diamine; **DITim**=3-[2-(1*H*-imidazol-4-yl)-ethylimino]-2-methyl-butane-2-thiol-11-ide; **Pypep**= *N*-[2-(1*H*-imidazol-4-yl)ethyl]pyridine-2-carboxamide-8-ide; **Prpep**=pyrimidine-4-carboxylic acid [2-(1*H*-imidazol-4-yl)-ethyl]-amide-8-ide; **$PaPy_3$**=*N*-{2-[bis(pyridin-2-ylmethyl)amino]ethyl}pyridine-2-carboxamide-18-ide; **$PaPy_2O$**=*N*-{2-[bis(pyridin-2-ylmethyl)amino]ethyl}-2-hydroxybenzamide-18,27-diide; **SEt**= ethanethiol-1-ide; **S_2-o-xyl**=1,2-phenylenedimethanethiol-8,10-diide; **SEtOH**=2-mercapto-ethanole-1-ide; **bpia**=(1-methyl-1*H*-imidazol-2-ylmethyl)-bis-pyridin-2-ylmethyl-amine; **$py_2(nMe)_2$**= 3,11-dimethyl-3,11-diaza-tricyclo[11.3.1.1^{5,9}]octadeca-1(16),5,7,9(18),13(17),14-hexaene.

[c] The solvents for which the redox potentials were measured are: ***W***: water; ***AN***: acetonitrile; ***DMF***: dimethylformamide.

[d] Since compound **13** exhibited maximum deviation from the measured redox potentials its contribution was ignored in the first step of the fitting procedure [described in the Results and Discussion part (0)] and considered only for the second step.

Table 2. Prediction set of 18 different TMCs for which redox reactions are considered in three different solvents [water (W), acetonitrile (AN), dimethylformamide (DMF)].

No.[a]	model compound [b]	solvent [c]	No.[a]	model compound [b]	solvent [c]
31$_i$	$[Fe(cyclamAc)(N_3)]^{2+/1+}$	**AN**	**40.**	$[Fe(tacnPy_2)(AN)]^{3+/2+}$	**AN**
31$_{ii}$	$[Fe(cyclamAc)(N_3)]^{1+/0}$	**AN**	**41.**	$[Fe(N_4Py)(Cl)]^{2+/1+}$	**AN**
32.	$[Ni(tacn)_2]^{3+/2+}$	**W**	**42.**	$[Fe(N_4Py)(AN)]^{3+/2+}$	**AN**
33.	$[Fe(dtne)]^{3+/2+}$	**W**	**43.**	$[Fe(Py_3tacn)]^{3+/2+}$	**AN**
34.	$[Ni(dtne)]^{3+/2+}$	**W**	**44.**	$[Ni(Py_3tacn)]^{3+/2+}$	**AN**
35.	$[Fe(terpy)_2]^{3+/2+}$	**DMF**	**45.**	$[Fe(TCTA)]^{0/1-}$	**W**
36.	$[Fe(SPh)_4]^{1-/2-}$	**AN**	**46.**	$[Ni(TCTA)]^{0/1-}$	**W**
37.	$[Fe(SCH_2CON(CH_3)_2)_4]^{1-/2-}$	**AN,DMF**	**47.**	$[Mn(TCTA)]^{0/1-}$	**W**
38.	$[Fe(S\text{-}i\text{-}Pr)_4]^{1-/2-}$	**AN**	**48.**	$[Fe(Pyr_2Py)_2]^{3+/2+}$	**AN**
39.	$[Fe(bpy)(CN)_4]^{3+/2+}$	**W**			

[a] Numbers in front are used to refer to specific TMCs in text.

[b] The total charges of the pairs of redox states are given as superscripts; for compound **31** the redox potential is measured for two different pairs of redox states; abbreviations for ligands besides those already mentioned in Table 1: **cyclamAc**=(1,4,8,11tetraaza-cyclotetradec-1-yl)-acetic acid anion; **dtne** = 1,2-di(1,4,7-triazonan-1-yl)ethane; **terpy** = 2,2':6',2''-terpyridine, **SPh** = benzenethiol-7-ide; **$(CH_3)_2NCOCH_2S$** = *N*,*N*-dimethyl-2-sulfanylacetamide-1-ide; **HS-*i*-Pr** = propane-2-thiol-1-ide; **tacnPy_2** = 1-(dipyridin-2-ylmethyl)-4,7-dimethyl-1,4,7-triazonane; **N_4Py** = 2,2-di(pyridin-2-yl)-N,N-bis(pyridin-2-ylmethyl)ethanamine; **Py_3tacn** = 1,4,7-tris(pyridin-2-ylmethyl)-1,4,7-triazonane; **TCTA** = 2,2',2''-(1,4,7-triazonane-1,4,7-triyl)triacetate; **Pyr_2Py** = 2,6-bis(3,4-dihydro-2H-pyrrol-5-yl)pyridine.

[c] The solvents for which the redox potentials were measured are: ***W***: water; ***AN***: acetonitrile; ***DMF***: dimethylformamide.

For the development of the approach, which will be described in this chapter, only the training set has been used. The prediction set was introduced at a later time to validate our approach more carefully. Since the same training set without any change of the parameters has been used, this test can be considered as a true blind prediction. While some of considered complexes have been known for a long time, others have been synthesized only within the last three decades[100-119]. Several of these complexes were synthesized to mimic commonly observed cofactors in proteins[104, 106-108, 110-112, 115, 116, 118, 119] as well as the metal-chelating part of bleomycin[105, 111, 112, 114].

The model compounds were selected systematically to include nitrogen, oxygen, sulfur, carbon and chlorine as coordinating atoms. These are the atoms, which are most frequently seen in the coordination sphere of the metal centers of protein cofactors. Similarly, the metal atoms of Fe, Mn and Ni, involved in the chosen transition metal complexes, are biologically most relevant. It is sufficient to mention, such important

biological systems, as photosystem I/II (Fe and Mn), hemoglobin (Fe), cytochromes (Fe) and hydrogenases (Fe and Ni), in which these metals are playing a crucial role.

Another criterion for the selection of the model compounds was the availability of experimentally measured reliable redox potentials (see also part 2.2). Model compounds, which demonstrate an irreversibility of the redox reaction pointing to larger conformational changes, were sorted out.

Since the computational costs are increasing with the number of atoms ($\sim N_{atom}^3$ for DFT), one was interested in relatively small compounds. The smallest available TMCs, which were considered (TMCs **1** and **25**) consist of 13 atoms. However, the rest of compounds are relatively large with number of atoms between 29 and 67 (see Figure 19).

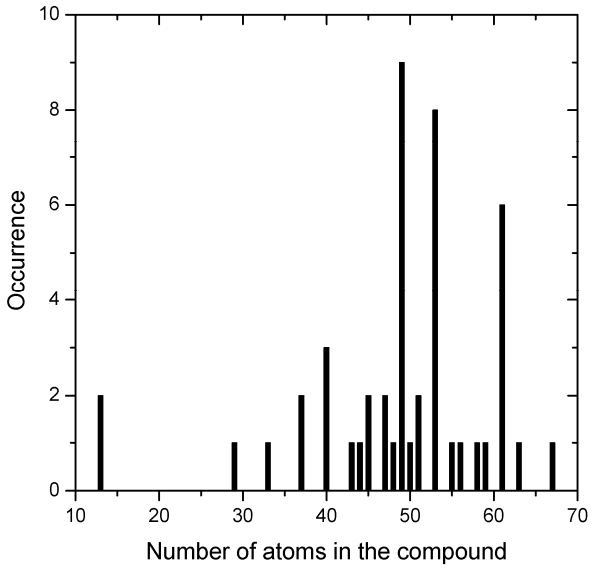

Figure 19. Diagram showing the occurrence of the model TMCs in our training and prediction sets dependent on the number of atoms.

3.1.2 Computation of redox potentials

The standard (°) redox potential $E°$ of the redox reaction $Ox_s + e_g \rightarrow Red_s$ in solution is given by

$$E^\circ = -\frac{\Delta G^\circ}{n \cdot F} = -\frac{\Delta G_s^\circ - \Delta G_{SHE}^\circ}{n \cdot F}, \qquad (3.1)$$

where ΔG°, ΔG_s° and ΔG_{SHE}° are, respectively, the standard Gibbs free energy of reduction relative to that of H^+ [standard hydrogen electrode (SHE)], the standard Gibbs free energy of reduction, and the Gibbs free energy of the redox reaction $H^+_{water} + e_g \rightarrow \frac{1}{2} H_{2(g)}$ at SHE. The Faraday constant is F = 23.06 kcal·mol^{-1}·V^{-1}, the number of transferred electrons in the redox reaction is n. Since in this study, only one-electron transfer processes are considered, the parameter n in Eq. (3.1) is equal to 1. In the paragraph 2.2.1, a number of methods, which suggest different values for the absolute potential of SHE, including numbers in the range from 4.2 V to 4.73 V[86-93] have been already mentioned. Since there is no general agreement on the absolute value of SHE so far, the value of 4.44 V recommended by IUPAC[86] was considered. Converting this redox potential value into energy one obtains $\Delta G_{SHE}^\circ = -4.44$ eV. It should be emphasized that the particular value of ΔG_{SHE}° used is not crucial for the B4(XQ3)LYP-approach, since the computed redox potentials can at the end still be adjusted to a different value of ΔG_{SHE}°.

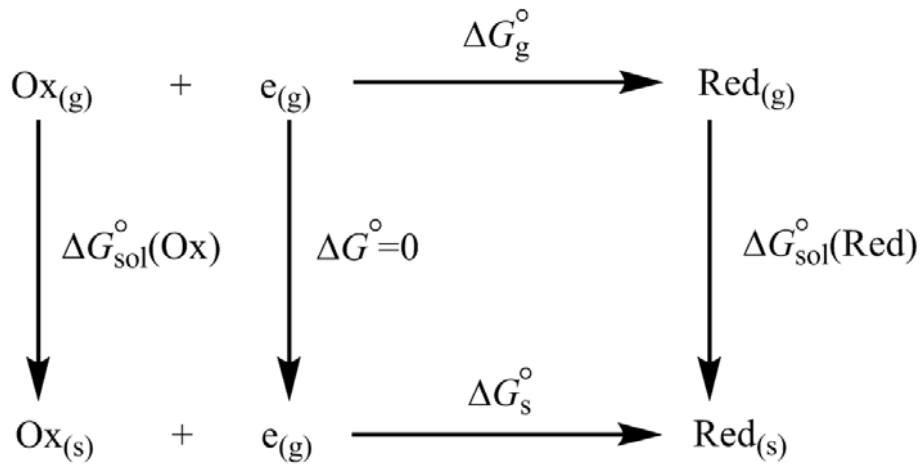

Figure 20. Thermodynamic cycle for the redox process.

The standard free energy of reduction ΔG_s° can be calculated routinely using the thermodynamic cycle[120, 121] describing the relation between the electron attachment process in vacuum [gas phase, (g)] and the corresponding reduction in solution (Figure 20).

The free energy of a specific redox state (Red or Ox) of TMC in solution is defined as

$$G_s^\circ = G_g^\circ + \Delta G_{sol}^\circ, \qquad (3.2)$$

where G_g° and ΔG_{sol}° are free energy in vacuum and free energy of solvation (see paragraph 2.1.2.3), respectively. Therefore, the free energy of a redox reaction in solution can be given as

$$\Delta G_s^\circ = G_s^\circ(\mathrm{Red}) - G_s^\circ(\mathrm{Ox}) = \Delta G_g^\circ + \Delta\Delta G_{sol}^\circ . \tag{3.3}$$

The free energy in vacuum can be calculated as follows

$$G_g^\circ = E_0 + \mathrm{ZPE} + \Delta G_{0\to 298\mathrm{K}} , \tag{3.4}$$

where E_0 is the ground-state electronic energy in vacuum, ZPE the zero-point vibrational energy and $\Delta G_{0\to 298\mathrm{K}}$ the thermal vibration free energy at 298 K. The values of E_0, ZPE and $\Delta G_{0\to 298\mathrm{K}}$ were calculated quantum chemically. The details of the quantum-chemical computations are given in paragraph 3.1.3.

3.1.3 Quantum chemistry

The quantum-chemical computations were done with the DFT method implemented in the program JAGUAR, version 5.5[122]. The JAGUAR package was chosen due to its high performance especially for the treatment of systems, containing transition metals.

The quantum-chemical computations performed in this study include the following three procedures (see Figure 21). First of all the geometries of the model compounds were optimized. Where the coordinates of the crystal structures were available, they were used as starting structures for the optimization; otherwise structures were created using the program Molden[123]. In all cases, geometry optimizations of the model compounds were performed in vacuum using the B3LYP functional with LACVP[124] effective core potential for transition metal atoms and 6-31G** basis functions for main group atoms (corresponding to LACVP**).

In the second step, single-point energies [E_0 in eq. (3.4)] for the computation of redox potentials were calculated for optimized geometries in vacuum, using the B3LYP and the newly introduced B4LYP (see below) functionals with large basis set LACV3P**++. This basis set includes the LACV3P[122] effective core potential for transition-metal atoms and 6-311++G** basis functions for all other atoms.

The optimized geometries were also used in the third step, where the vibrational frequency calculations were performed to obtain zero-point energies and vibrational correction to the free energies at 298K, $\Delta G_{0\to 298\mathrm{K}}$.

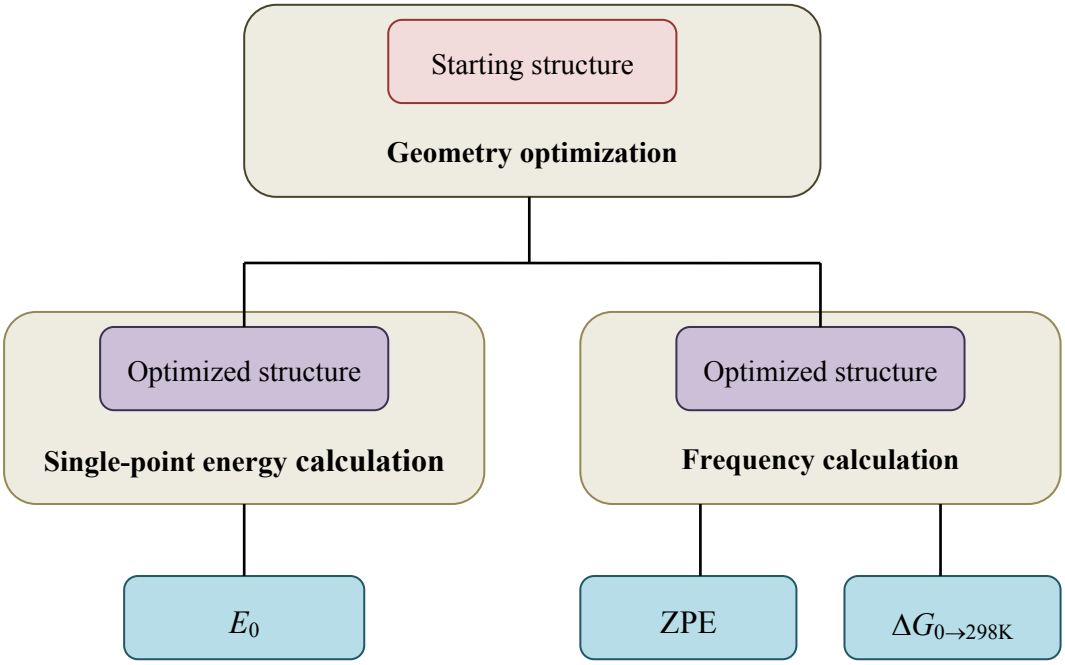

Figure 21. Diagram representing quantum-chemical computations, necessary for obtaining of the energy data, entering eq. (3.4).

For these computations the B3LYP functional combined with the LACVP** basis set was used. No scaling of frequencies was applied, since its effect would be very smallin the energy differences between reduced and oxidized states. The considered model compounds can have different spin states (as already explained in the part 2.3). Therefore, both low- and high-spin states for the reduced and oxidized complexes were included in the computations. Moreover, as it will be shown in part 4.1, one of the development steps of the B4(XQ3)LYP-approach is directly related to the problem of spin states of the TMCs. For open shell systems unrestricted DFT was used. To explore how the spin multiplicity of the electronic ground state is reproduced using specialized DFT methods, the single point electronic energies were computed with B3LYP*[21] and X3LYP[125, 126] functionals for some TMCs (see Table A4-5 of appendix).

3.1.4 B4XLYP hypothesis. Introduction of the B4(XQ3)LYP-approach

The B4XLYP hypothesis, which will be described in the following, is the central idea of our study. It is indeed very simple and suggests a new four-parameter hybrid functional B4XLYP (hypothetical functional), which can be obtained by rewriting the B3LYP functional as follows

$$E_0^{\mathrm{B4XLYP}} = \hat{a}_0 E_x^{\mathrm{exact}} + (1-a_0)E_x^{\mathrm{LSDA}} + E_x^{\mathrm{X}} + a_x \Delta E_x^{\mathrm{B88}} + a_c E_c^{\mathrm{LYP}} + (1-a_c)E_c^{\mathrm{VWN}} . \quad (3.5)$$

In this functional, $\hat{a}_0$ is an additional variable parameter for the exact exchange term, E_x^{exact}, differing from a_0 the parameter for E_x^{LSDA} that remains at the standard value of 0.20. Thus introducing $\hat{a}_0$ one decouples the parameters of exact exchange E_x^{exact} and local exchange E_x^{LSDA}, used for the standard B3LYP functional [Eq. (1.1)]. The parameter adjustment yields $\hat{a}_0$ obeying $0 < \hat{a}_0 < a_0$. Setting of this condition leads to a decreased weight of E_x^{exact} in the functional. To compensate for decrease of the exact exchange contribution and possible deficiencies of the B3LYP functional an additional term E_x^{X} of yet unknown form (abbreviated as X in the notation B4XLYP) is introduced. As long as E_x^{X} has not been specified explicitly the expression (3.5) involves four parameters. The parameters (a_0, a_x, a_c) adopt the same values as in the B3LYP functional, such that for $\hat{a}_0 = a_0$ and E_x^{X}=0 one regains the B3LYP functional. As long as the E_x^{X} part is unknown the B4XLYP functional remains hypothetical and cannot directly be used for the computation of electronic energies. Nevertheless, the B4XLYP hypothesis can be validated indirectly for certain properties of transition metal complexes as described in the following.

It is assumed, that the influence from the unknown E_x^{X} can be accounted for by first computing the electronic ground state energies with the incomplete four parameter functional B4LYP (B4XLYP without E_x^{X})

$$E_0^{\mathrm{B4LYP}} = \hat{a}_0 E_x^{\mathrm{exact}} + (1-a_0)E_x^{\mathrm{LSDA}} + a_x \Delta E_x^{\mathrm{B88}} + a_c E_c^{\mathrm{LYP}} + (1-a_c)E_c^{\mathrm{VWN}} \quad (3.6)$$

and adding an appropriate empirical correction term G_X afterwards. For convenience, the whole machinery is called the **B4(XQ3)LYP-approach**. Abbreviation (XQ3) points at the character of the correction term G_X, which in our applications is a function of the charge of the redox-active complex and involves three additional parameters (see details in paragraph 4.2). Thus, the free energy in vacuum, which is computed is a combination of quantum-chemical and empirical parts:

$$G_g^{\circ,\mathrm{B4(XQ3)LYP-approach}} = E_0^{\mathrm{B4LYP}} + \mathrm{ZPE} + \Delta G_{0\rightarrow 298\mathrm{K}} + G_X \;=\; G_g^{\circ,\mathrm{B4LYP}} + G_X \; . \quad (3.7)$$

The correction G_X is determined by fitting a third-order polynomial $G_X(q)$ (involving four coefficients) in the total charges q of the reduced states of the considered TMCs to optimize the agreement between calculated and measured redox potentials. To evaluate redox potentials, energy differences involving $G_X(q)$ - $G_X(q+1)$ are considered. Note, that in these differences the constant term of the polynomial $G_X(q)$ cancels. Hence, the

correction term involves three additional parameters such that for the B4(XQ3)LYP-approach a total of seven parameters are used from which three parameters adopt the same values as in the B3LYP functional. In the procedure to determine the coefficients of the polynomial $G_X(q)$, 30 different TMCs of the training set (Table 1), were considered (see below for more details). It should be noted here that the B4LYP functional is incomplete and can therefore not be used for geometry optimization for which exclusively the B3LYP functional is used. With $\hat{a}_0 = 0.12$ ($a_0 = 0.20$) in eq. (3.6), used to compute redox potentials of transition metal complexes, the B4LYP DFT functional reproduces correctly the experimental spin multiplicities of the electronic ground states for the studied compounds. This is in analogy to the B3LYP* functional[21], which corresponds to the parameter values of $\hat{a}_0 = a_0 = 0.15$ in eq. (3.6). Except for TMCs **13, 16** and **18** the B3LYP* functional yields for the free energies in dielectric medium G_s° , eq. (3.3), the proper spin multiplicity (Table 3) (See paragraph 4.1 for more details.)

3.1.5 Generation of atomic partial charges

Since the procedure involves computations of electrostatic solvation energies, one needs appropriate atomic partial charges. In paragraph 2.1.3 some common strategies for the generation of atomic partial charges were already represented. Using the strategy, which is the most appropriate for the given TMC system is an important point. In the following details of the procedure used in B4(XQ3)LYP-approach are given to generate atomic partial charges.

Atomic partial charges were determined from the electrostatic potentials derived from the molecular electronic wave functions. The necessary quantum-chemical computations were done in vacuum at the B3LYP/LACVP** level of theory using JAGUAR 5.5[122]. Electrostatic potentials were calculated on a grid formed by merging sets of spherical shells with centers located on the atomic nuclei, with no grid points within the molecular vdW surface. The values of the vdW radii used by the program Jaguar 5.5[122] for electrostatic potential computation were used as is (H 1.597 Å, C 1.949 Å, N 1.831 Å, O 1.702 Å, S 2.070 Å, Cl 1.958 Å, Fe 1.456 Å). These electrostatic potentials were used in the RESP[65, 77] two-step procedure, which fits the quantum chemically calculated electrostatic potential with an atom-centered point-charge model (for details see paragraph 2.1.3). The charge fitting was performed in two stages using hyperbolic restraints with the total charge fixed. In the first stage of the RESP procedure the atomic charges were allowed to change with a restraining weight of a = 0.0005 a.u. [Eq. (2.50)]. In the second stage charges on hydrogen atoms and their neighbor atoms were left free while all other atomic charges were constrained at their values obtained from the first stage using a restraining weight of a = 0.001 a.u..

3.1.6 Computation of solvation energy

For the computation of solvation energy ΔG°_{sol} the solvent was represented as dielectric continuum, with dielectric constants of $\varepsilon_w = 80.0$, $\varepsilon_{AN} = 37.5$ and $\varepsilon_{DMF} = 36.7$ for water, acetonitrile (AN) and dimethylformamide (DMF), respectively[127]. The solvation energies were computed with the program SOLVATE from the MEAD program suite[53, 54] by solving the Poisson equation numerically by a finite difference method. In this approach, the solute is represented by a set of atomic point charges embedded in the solute cavity with dielectric constant $\varepsilon = 1$. Outside the solute cavity, a dielectric constant appropriate for the solvent was taken and the ionic strength was set to zero. The boundaries of the solute are defined by the molecular surface using atomic radii for the solute atoms with a solvent probe radii of 1.4 Å, 2.23 Å and 2.54 Å for water, AN and DMF, respectively. These solvent probe radii of AN and DMF were estimated by the probe-radius calculator implemented in the program JAGUAR, which determines the probe radius according to molecular weight and density of the solvent[122]. Optimized geometries were used for the computation of solvation energies. The implicit-solvent model in the electrostatic calculations represented by probe radii and dielectric constant ignores specific properties of the solvent, which in turn influence the solute cavity. To account for these effects in the solvation model different sets of solute atomic radii for different solvents were used, following previous workers[12, 14, 128]. The solute atomic radii for each solvent were optimized to obtain in combination with B4LYP and the ΔG_X correction the best agreement between calculated and measured redox potentials (see part 0). As a starting set for the optimization the Bondi atomic radii[129] were used. These are in Å for H, C, N, O, Cl, and S: 1.2, 1.7, 1.55, 1.52, 1.75 and 1.8. Since the transition metal atom is situated in the center of the complex, buried by ligand atoms, its atomic radius practically does not contribute to the surface of the complex. Therefore, its radius was not optimized, leaving the value of 1.456 Å (Fe), 1.480 (Mn) and 1.417 (Ni) from the JAGUAR data set unchanged[122]. The two-step focusing procedure was used to solve the Poisson equation on a grid consisting of $(189)^3$ points, using first a low- and then a high-resolution grid with lattice constants of 0.4 Å and 0.1 Å, respectively.